Mineralization of soil organic matter from equatorial giant podzols submitted to drier pedoclimate: A drainage topochronosequence study

Célia R Montes, Patricia Merdy, Wilson T.L. da Silva, Débora Ishida, Adopho J Melfi, Roberta C Santin, Yves Lucas

Mineralization of soil organic matter from equatorial giant podzols submitted to drier pedoclimate: a drainage topochronosequence study

Célia R. Montes[a], Patricia Merdy[b], Wilson T.L. da Silva[c], Débora Ishida[a], Adopho J. Melfi[a], Roberta C. Santin[d], Yves Lucas[b*]

[a] IEE, NUPEGEL, Universidade de São Paulo, São Paulo 05508-010, Brazil

[b] Université de Toulon, Aix Marseille Université, CNRS, IM2NP, 83041 Toulon CEDEX 9, France

[c] Embrapa Instrumentation, São Carlos 13560-970, Brazil.

[d] CENA, Universidade de São Paulo, Piracicaba 13400-970, Brazil

*Corresponding author (lucas@univ-tln.fr)

Hightlights

- Active hydromorphic podzol in the area store around 63 kgC m^{-2}
- Erosive incision by a river meander resulted in air entry and oxygenation of the Bh
- C content in the Bh of a podzol truncated due to meander diminished by 70%
- Drier climate would induce C emission from Amazonian podzol Bhs

Abstract

Podzol soils are an important carbon pool in the Amazon, due to the high organic matter (OM) content in their topsoil horizons and deep Bh. To quantify the evolution of the stock and the lability of this carbon pool in the hypothesis of the onset of drier climates, we studied a soil toposequence at the end of which the incision of a river meander lowered the water table, as would result from a drier climate, allowing oxidation the Bh horizons. The soil OM was quantified and characterized (physical fractionation, humification indexes, ^{14}C average age) and its lability under oxic conditions was estimated by measuring respiration during a 660-days experiment. Podzol genesis time was calculated by constraining the carbon fluxes using both C stock and ^{14}C average age. The results confirmed that the studied podzols store large amounts of carbon (62.8 kgC m^{-2} on average). They resulted from a long genesis time, probably greater than 30-50 ky. Topsoil OM is very labile with a residence time of about 100 y; Bh OM is highly humified with a high C/N (62.7 on average) related to low respiration rates. The measured respiration rates were used to estimate the C emission that would result from drier climates at 55 gC m^{-2} y^{-1} on average during the first 100 y, which would correspond, by extrapolation, to 8.5 10^{12} gC y^{-1} for all Amazonian podzols.

Keywords: Amazon podzol; Soil organic matter; Humification index; Soil carbon storage and loss; Climate change; Soil formation rate

1. Introduction

Equatorial podzols are characterized by upper organic matter (OM)- rich horizons and thick sandy eluviated horizons (E horizons, also called white sands) overlying deep OM-rich horizons called Bh. In these soils, the dissolved organic matter (DOM) produced in the topsoil is transferred at depth, through the E horizons, by the percolating waters (Lucas, 2001). Part of this DOM is directly exported to the river network by the lateral flow of the groundwater perched on the Bh horizons and circulating in the E horizons. The other part enters the Bh horizons where it can be immobilized as soil organic matter (SOM), remobilized in the perched groundwater (Bardy et al., 2011), mineralized by microbial activity or transferred towards deeper horizons and deep groundwater (Lucas et al., 2012).

Despite their very low fertility, equatorial podzols are of interest because, on the one hand, they release large amounts of dissolved organic carbon (DOC) in the river sytem (Leenheer, 1980), most of which is transferred to the sea, participating to the storage of carbon on the scale of geological time (Tardy et al., 2009). On the other hand, since most of them are giant podzols compared to podzols of cold regions, i.e. with E or Bh horizon thicknesses that can reach

several meters, they store large amounts of carbon in their upper and Bh horizons: hydromorphic podzols can store more than 100 kgC m^{-2} in the whole profile and more than 80 kgC m^{-2} in the only deep Bh (Montes et al., 2011). These soil systems therefore contribute significantly to the global CO_2 cycle (Marquez et al., 2016, 2017). The dynamics of DOM transfer and SOM accumulation, however, are still poorly understood.

Carbon accumulation in deep Bh horizons is due to the acidic and water-saturated conditions found there. It should be noted that in most areas the hydromorphic podzols are not situated in the bottom of valleys but in a plateau position or on slopes, higher than the phreatic base level (Lucas et al., 1987). As the Bhs have low hydraulic conductivity, they support a perched water-table that joins the deep water-table in restricted parts of the landscape. As a result, the upper part of the Bh is always in waterlogged conditions, which prevents the entry of air from the E horizon into the Bh (Ishida et al., 2014), It can be drained if the climate turns drier, allowing oxygenation of the underlying Bh. For the Upper Rio Negro Basin, where most of the Amazonian podzols are found, climate change modelling predictions point to the gradual onset of a drier season centered around October (Gutiérrez et al., 2021; Iturbide et al., 2021). The CMIP6 model predicted a negligible decrease in annual rainfall, but an increase in the number of consecutive dry days. These were on average 15 days during the 1986-2005 reference period; forecasts were 19 and 31 days for SSP2, near-term period (2021-2040) and SSP5, long-term period (2081-2100), respectively. The CORDEX South America model predicted no change for either scenarios; the CORDEX Central America model predicted 28 and 39 days

113 respectively. An increase in the number of consecutive dry days
114 would alter the dynamics of the water tables perched on the Bh,
115 which could temporarily disappear, allowing air to penetrate into
116 OM-rich horizons that are generally waterlogged. This can lead to
117 increased C mineralization through better aeration satisfying the O_2
118 demand of microorganisms. Increased in dry/wet cycles is also likely
119 to have an impact on the mineralization of C: rewetting of the soil
120 after a period of drying has long been known to cause a burst of
121 respiration (Birch, 1958), so that dry/wet cycles can accelerate soil C
122 loss relative to what would be lost under constant conditions (Miller
123 et al. 2005). Tadini et al. (2018) showed significant compositional
124 changes in the humic acid (HA) fractions of Bh SOM throughout the
125 horizon, with four types of organic matter: recalcitrant, humified, and
126 old dating; labile and young dating; humified and young dating; and
127 little humified and old dating. This suggests a different sensitivity of
128 these organic matters to mineralization processes.
129 In such a context, a first objective of the present work was to
130 evaluate the sensibility to mineralization of the OM issued of
131 hydromorphic podzols to predict the kinetics of CO_2 release after
132 oxygenation.
133 Another way to evaluate the evolution of podzolic OM in a
134 context of climate change is to study a chronosequence where the
135 hydromorphic podzols were progressively submitted to a drier
136 pedoclimate. Two types of such chronosequence can be identified:
137 (1) a Bh formed beneath permanent water table then was submitted to
138 alternating dry and wet conditions due to an external change in
139 drainage conditions and (2) podzols were formed under humid
140 climates then subjected to dryer climates. We have identified in the

Amazon a topochronosequence of the first type, for which the change in drainage conditions was a lowering of the water table caused by the erosive incision of a river. The second objective of the present study was therefore to compare the rates of Bh mineralization along this topochronosequence.

2. Material and methods

2.1. Study area and sampling

The study area is situated in Brazilian Amazonia, north of the city of Barcelos, at the edge of the Demini River at the central coordinates 0°17'30"N and 62°48'0"W (Fig. 1). Landscape is a flat area whose altitude is 3 to 15 m over the Demini River higher level. Annual rainfall is around 2600 mm (Reboita et al., 2010) without a marked dry season. The geological substratum, previously considered as a part of the Içá sedimentary formation (Reis at al., 2006), was more recently reclassified as late Pleistocene (129 to 11.7 ky BP) Rio Negro – Rio Branco sedimentary formation, that mainly consists in unconsolidated sands with some clay-silt and conglomerate layers (IBGE, 2011). These sediments were deposited as a megafan following the slow subsidence of the Guyana Shield, giving the largest wetland area of the Amazon (Cremon et al., 2012). After these authors, the studied soils are located on one of the oldest deposit of the megafan whose age, however, is not precisely known. Soils in the area are mainly typical tropical podzols and hydromorphic podzols

(Lucas et al., 1996; Dubroeucq and Volkoff, 1998; Montes et al., 2011) associated to some ferralsols which can occur occasionally on scattered hills 2 to 10 m higher than the flat, hydromorphic podzolic inter-hill surface (Pereira et al., 2015). The forest on well-drained podzols is a forest of tall trees, but with low species diversity (Adeney et al., 2016; García-Villacorta et al., 2016); over the hydromorphic podzols is a specific vegetation named campinarana, characterized by a high density of smaller trees (20 to 30 m) that are adapted to physiological stress caused either by waterlogging when the water table is near the surface, or by drought when the water table is further from the surface (Anderson, 1981). In the lowest areas which are always waterlogged, hydromorphic podzols are observed under an herbaceous vegetation forming clumps 20-30 cm high, with the presence of bare patches of white sand.

The study area was chosen on the convex side of a meander of the Demini River (Fig. 1), out of the meandering channel in an area where erosion cut directly in the Rio Negro – Rio Branco sedimentary formation, in order to observe the podzol evolution after the lowering of the water table related to the river incision.

Soils were studied and sampled by the mean of hand-auger drilling, using casing in the E horizons to avoid sand collapsing in the borehole. Samples for microbial respiration measurements were maintained in the dark at temperature below 5° until analyzed, which occurred within 2 weeks, such a procedure was shown not to affect respiration measurements (Lucas et al., 2020). Samples for soil organic matter (SOM) characterization were frozen and maintained frozen until analyzed. Undisturbed samples for bulk dry density were

taken in boreholes by hammering a cylindrical Ø 3 cm piston sampler.

2.2. Laboratory characterizations

2.2.1. Soil characterization

Soil particle size distribution was performed using the Robinson pipette method. Total organic carbon (TOC) was determined using a LECO CR-412 TOC analyser. No carbonates minerals were found in these very acid soils (pH<5) so that in the following "C content" refer to "organic C content". A SOM humification index (H_{LIF}) was obtained by Laser Induced Fluorescence Spectroscopy (LIFS) after Milori et al. (2006): the bulk sample grinded to pass a 250-µm mesh was pressed in pellets and the fluorescence emission spectra between 420 and 800 nm under a 405 nm excitation was obtained using a Hamamatsu photomultiplier. The H_{LIF} index was calculated dividing the area of the LIF spectrum by the C content of the sample.

The HA fractions were isolated and characterized in a previous work (Tadini et al., 2018) using the procedure recommended by the International Humic Substances Society (Swift, 1996). Here we used the humification index (A_{465}) of HA determined as the total area under the fluorescence emission spectrum recorded at the excitation wavelength of 465 nm (Milori et al., 2002).

All mineralogical determinations were performed after organic matter removing with H_2O_2. Main minerals were identified by XRD (X-ray diffraction) of Cu Kα radiation on powder samples using a Philips PW 1877 diffractometer. Kaolinite and gibbsite were

confirmed by FTIR (Fourier-transformed Infra-Red spectrometry) on sample-KBr pellets using a Shimadzu IR Prestige-21 spectrometer. Differential thermal analysis (DTA) and thermogravimetric analysis (TGA) were undertaken with a DTG-60H-Simultaneous DTA-TG (Shimadzu, Kyoto, Japan).Goethite was identified using the 488 and 413 nm absorption bands (Scheinost et al., 1998) by DRS (Diffuse Reflectance Spectroscopy, Varian Cary 5 spectrometer)

Saturated hydraulic conductivity (K_{sat}) was measured on undisturbed samples taken with a Ø 37 mm piston sampler hammered in boreholes. Samples were sealed in a polycarbonate tube, led to water saturation by a 24-h progressive rise of water level from the base of the cylinder, then remained 48 hours for dissolution of the air possibly trapped in the porosity. The water used was previously brought to pH 4 (Lucas et al., 2012) with H_2SO_4 to avoid any dispersion of the organic matter likely to modify the value of K_{sat}.

Physical fractionation of the organic matter was realized in triplicate using the procedure described in Sohi et al. (2001). Five grams of soil sieved at 2 mm were placed in centrifuge bottles containing 35 mL of 1.8 g cm^{-3} $NaIO_3$ solution, manually stirred during 30s then centrifugated at 8000 g during 30 mn. The floating particles, that corresponded to the light free fraction (LFF), were separated by filtration on a GF/A 1.6 µm filter. The filtrate was returned to the corresponding centrifuge bottle containing the soil residue and sonicated. Floating particles corresponded to a light intra-aggregate fraction, the light occluded fraction (LOF), they were separated by centrifugation and filtration as for LFF. The OM remaining in the centrifugation pellet corresponded to the heavy

fraction (HF). C on the filters and on the final centrifugation pellets was quantified as for TOC.

2.2.2. Basal respiration

Soil respiration was determined using the method described in Paul et al. (2001). The respiration gas samples were analyzed for CO_2 concentrations using a GC-17A Shimadzu gas chromatograph equipped with a flame ionization detector. After extraction, jars were opened for 5 mn for equilibrating with external atmosphere. Sampling was done twice a week during the 2 first weeks, then thrice a week until 3 months, then weekly until 4 months, then monthly until the end of experiment that was stopped after 660 days. Detailed data are given in supplementary material; they were used to calculate the cumulative respiration during the 660 days long experiment and the SOM respiration rates using a 2 pools model, each pool having a first order kinetics. The respiration curves were fitted by the Excel Solver using the Evolutionary algorithm to find the parameters values that minimized the normalized root mean square deviation (RMSD). Examples of respiration curves and processing are given in Lucas et al. (2020).

2.2.3. Isotopic measurements

After freeze drying, soil samples were ground to pass a 106-µm mesh. Between 35 to 90 mg of the sample, depending on carbon concentration, was transferred to a tin capsule for elemental and isotopic analysis. The isotope ratios of carbon ($^{13}C/^{12}C$) and nitrogen ($^{15}N/^{14}N$) of each sample were determined using a continuous-flow isotope ratio mass spectrometer (Delta Plus, ThermoFisher Scientific,

Bremen, Germany) coupled to an elemental analyzer (CHN-1110, Carlo Erba, Rodano, Italy). Carbon and nitrogen isotope compositions were calculated as:

$$\delta\ (‰) = [(R_{sample}/R_{standard}) - 1] \times 1000$$

where R is the ratio of $^{13}C/^{12}C$ or $^{15}N/^{14}N$. Stable isotope ratios for C were measured using internationally standard PDB (Limestone from the Grand Canyon region, USA) while the standard for nitrogen was atmospheric air.

2.2.4. Radiocarbon measurement

Radiocarbon measurements were carried out at the Poznań Radiocarbon Laboratory, Poland. Radiocarbon dating of organic matter must be corrected for "bomb carbon", the atmospheric ^{14}C peak brought by the tropospheric nuclear tests of the 1960s (Trumbore, 2000). In the Bh, we assumed that the proportion of bomb carbon in the Bh organic matter was negligible and we calculated a conventional, uncalibrated age from the radiocarbon pMC (percent modern carbon) value. This age is an apparent age because the Bh are open systems mixing organic carbon of different ages. The topsoil organic matter, however, was very younger and had a significant amount of post-bomb carbon, giving a pMC higher than 100 %. In such case, we assumed that the topsoil horizons reached a steady state before 1950 and calculated an apparent age using the method given in Doupoux et al. (2017).

307 *2.3. Statistical analysis and modelling*

308 Statistical analysis was performed using XLSTAT2017. We chose
309 a correlation-type PCA on standardized variables to avoid sensitivity
310 to the scaling of the variables. Modelling was realized using the
311 method developed in Doupoux et al. (2017), in which the podzol
312 profile genesis time is constrained by both total carbon and
313 radiocarbon. For a given C pool, assuming a constant input of C and
314 a constant rate for C outflow, the relationships between total carbon
315 and radiocarbon can be calculated analytically. This allows the
316 calculation of the minimum time required to form the carbon pool.
317 The authors applied this method to give an estimate of the minimum
318 time required to form a given profile by considering three carbon
319 pools: a topsoil C pool and two pools in the Bh: a fast Bh pool (high
320 C turn-over) and a slow Bh pool (low turn-over).

321 The model required knowing the radiocarbon and total carbon
322 values in each pool. Total carbon was calculated from carbon weight
323 % and bulk density. Radiocarbon and carbon % were measured; the
324 bulk density was measured for some samples and, for the others,
325 estimated using the following equation proposed by Pereira et al.
326 (2016):

327

328 $\rho_p = 1.463 + 0.1998 \tan[1.044 - 0.002\ (clay)] \cos[0.125 +$
329 $0.135(C/N) + (3.543\ 10^{-5})\ (silt)^2 - 0.013\ (silt)] \cos[0.004\ (fine\ sand)$
330 $\cos(0.315 + \tan[0.005\ (clay) - 2.317)] - 1.065 \cos[0.315 + \tan(0.005$
331 $(clay) - 2.317])] - 0.144\ (total\ N)$

332

where *clay*, *silt*, *fine sand, C, N* and *total N* are expressed in g kg^{-1}. Total carbon stock as well as apparent ^{14}C age was calculated using linear interpolation between sampled depth.

3. Results and discussion

3.1. Soils description and main characteristics

The soils presented and discussed here (BAR1 to BAR6) are located in Fig. 1. The BAR1, BAR2 and BAR4 soil are situated on a toposequence (Fig. 2) starting from a waterlogged zone, in which the water table is all the time near or above the soil surface, until at the bank of the Demini River. BAR3 is in a position equivalent to that of BAR2 (Fig. 1), but in a more hydromorphic zone characterized by Campinarana-type forest and "murundus" micro-relief, i.e. earth mounds, about 0.6 m high and 2-10 m wide, separated by U-shaped channels, as described in Ishida et al. (2014). Soils BAR5 and 6 are located further towards the centre of the highly hydromorphic area, which is waterlogged most of the year (Fig. 1). BAR1 to BAR4 soils have been studied analytically in detail; all laboratory analysis are given in Supplementary material (Tab. S1).

All the soils were sand to loamy sand over the whole profile, except BAR1 mainly sandy loam, and BAR3, sandy loam in the upper part of Bh (Fig. 3). In all soils, apart from a few heavy minerals as zircon and ilmenites, the identifiable minerals were quartz, kaolinite, gibbsite and goethite (Fig. 4). In all E horizons,

quartz was the only mineral observed. Kaolinite was observed in trace amounts (<0.5%) in other horizons and in quantifiable amounts at depth. Goethite and gibbsite were observed at depth in BAR1 and along the whole profile in BAR4.

The upper soil horizons varied according to local waterlogging conditions. In the mostly waterlogged areas (BAR1, BAR3, BAR5 and BAR6), the surface horizon was a sticky, very fine-grained black peat (P horizons). In better drained areas, it was an A horizon. E horizons were well expressed and light in color (grey to light grey) except for BAR1, where it was weakly expressed, and BAR4, where it was absent. In the Bh horizons the C content ranged between 0.25 and 3.28 % (average 1.09%), unrelated with soil colour darkness (hue) (Munsell, 1990). The C content varied with depth but was higher in the upper indurated part of BAR2 and BAR3 Bhs. Considering all Bhs together, there was surprisingly no correlation between C content and clay, silt, (clay + silt) or kaolinite content (R^2 values < 0.13), while several studies point to the role of absorption on clay and oxide surfaces in immobilization of DOM (Kaiser and Zech, 2000; Merdy et al., 2021). Considering the soils separately, however, a correlation was observed between C content and clay content for BAR2 and BAR3 soil (R^2 equal to 0.56 and 0.50, respectively) and between C content and silt content in the BAR1 soil (R^2 equal to 0.39), which indicates that in these sandy materials the SOM tends to accumulate at the finest grain size levels.

A perched water table was observed above the Bh in the BAR2 and BAR3 soils. The saturated hydraulic conductivity K_{sat} was determined on three samples from the upper part of the BAR3 Bh (at 165-170 cm depth for each sample). The results gave a very low

388 average value ($7.7\ 10^{-9} \pm 2.3\ 10^{-9}$ m s^{-1}), which corresponds to an
389 impervious material, in accordance with the presence of perched
390 groundwater. A hydrogen sulfide odor, indicating reducing
391 conditions, was detected during drilling of the Bh horizons of all
392 profiles except BAR4.
393 BAR2 and BAR3 soils are typical giant equatorial podzols, with a
394 bleached sandy E horizon more than 1 m thick overlying a thick Bh.
395 In areas that are mostly waterlogged, podzols profiles are either
396 thinner (BAR5 and BAR6 soils) or less developed, such as BAR1
397 soil where the E horizon is not bleached, probably because the lateral
398 throughflow of the perched groundwater is slower. In the BAR4
399 profile, the E horizons and the indurated upper part of the Bh have
400 been removed by erosion due to the meanders of the Demini river.
401 The % carbon in the topsoil horizon as well as in the Bh are
402 significantly lower than in the BAR2 and BAR3 profile, indicating
403 that profile truncation likely resulted in a loss of carbon throughout
404 the profile. It should be noticed that the horizon situated beneath the
405 Bh was not reached for the BAR2 and BAR3 profiles despite the
406 casing of the borehole: the groundwater sapping in depth resulted in
407 the rise in the borehole of a mixture of groundwater and Bh material.
408
409
410 *3.2. Soil organic matter*
411
412 *3.2.1. Fractionation and humification indexes*
413 The results of the organic matter fractionation of the BAR1,
414 BAR3 and BAR4 soils are given in Fig. 5. Uncomplexed OM (LFF
415 and LOF fractions) is usually considered as a transient pool between

undecomposed litter and mineral-associated OM (HF fraction), with the turnover of LFF and HF respectively being the faster and the lower (Christensen, 2001). Here the highest LFF percentages were observed in the topsoil horizons and decreased in the top 50 cm while the LOF and HF percentages increased, indicating progressively stronger bonds with mineral material, although it was very sandy. In these horizons, a strong negative correlation was observed between LFF and LOF (Fig. 6), suggesting that LFF transformed into LOF with depth. In BAR1 and BAR3 Bhs, the HF percentage in SOM increased rapidly with depth, up to more than 70% around 2 m in depth, then gradually decreased. The positive correlation between LFF and LOF in BAR1 suggests that these fractions were both transformed to HF in the upper 2 m of Bh, and both produced from HF or brought by percolating solutions or deep groundwater to the transition towards the C horizon. A part of the highly humified OM can however appear in the LFF fraction (Cadisch et al., 1996). In BAR4 Bh, the SOM fractions are from 50 cm depth similar to those observed at depth in BAR3 Bh, which is consistent with the hypothesis of a truncated soil.

There was no significant correlation between the humification index A_{465} (Tadini et al., 2018) and any of the LFF, LOF and HF fractions, indicating that aromaticity was not related to a specific fraction. The A_{465} index was however higher in the BAR4 soil than in other soils, which indicates that since the lowering of the water table, the less aromatic compounds have been preferentially leached or mineralized.

Considering all the samples, there was no correlation between the H_{LIFS} index and the A_{465} index (Table 1). As pointed out by Tadini et

al. (2018), this is probably due to fluorescence self-absorption of dark Bh samples and these authors proposed a colour-corrected index (H_{LIFS-M}) calculated by dividing the H_{LIFS} index by the Munsell colour value of the bulk sample. The correlation, however, was also very weak between the colour-corrected index H_{LIFS-M} and the A_{465} index (Table 1). By gradually restricting the sample population to samples belonging to narrower colour range, the correlations between H_{LIFS} and H_{LIFS-M} indexes and the A_{465} index become progressively higher: R^2 between H_{LIFS-M} and A_{465} was 0.79 when considering only samples with a colour value <4. This indicates that the H_{LIFS} signal is indeed dependent on the degree of humification, but that the colour interference masks this dependence: black material lowered the fluorescence signal by absorption when white material exhausted the fluorescence signal by diffusion. The correction proposed by Tadini et al. (2018) was insufficient for our sample set. Pending the development of an effective correction, it is therefore advisable to restrict the use of the H_{LIFS} or H_{LIFS-M} indexes to samples belonging to a restricted colour range.

Table 1

Pearson coefficient of determination R^2 between A_{465} index and H_{lifs}, H_{LIFS-M} indexes

	H_{LIFS}	H_{LIFS-M}
All samples (n = 20)	0.06	0.12
Samples with colour value <5 (n = 13)	0.47	0.73
Samples with colour value <4 (n = 11)	0.65	0.79

3.2.2. Apparent age, C/N, respiration and isotopic data

The SOM of all topsoil horizons had a low apparent ^{14}C age (<110 y), indicating an average C turnover around 100 y (Trumbore, 2000), and a C/N < 25 (Fig. 7). Cumulative respiration was very high for the more hydromorphic P horizons (BAR1 and BAR3). In the well-expressed E horizons (BAR2 and BAR3), ages ranged from 205 to 830 y, C/N from 32 to 37 and cumulative respiration was high. In the Bh horizons, the apparent ages were variable but all high, ranging from 2510 to 9980 y. The C/N was higher than 40 (62,7 cm on average) in all the Bhs of untruncated podzols, that is to say profiles BAR1, -2, -3 where the water table have not been lowered. In BAR4, it ranged from 21 to 31. There were no significant differences between the profiles for $\delta^{13}C$, which increased slightly with depth, whereas the values of $\delta^{15}N$ were more discriminating with higher values for the BAR4 whole profile and the BAR2 topsoil (Fig. 8).

A principal component analysis (PCA) was performed on all the parameters discussed above, to which were added the values of the N % in the SOM humic acid fractions (%N HA, data from Tadini et al., 2018) (Fig. 9). It showed a positive Pearson correlation (R > 0.65) between ^{14}C age, A_{465} index, depth, $\delta^{13}C$ on one side and between N(%), %N HA on the other, the variables from one group having negative correlations (R < -0.65) with those from the other group. It also showed a very negative correlation between $\delta^{15}N$ and C/N.

These relationships indicate that, on the one hand, the increase in age is related to the increase in aromaticity and $\delta^{13}C$ and the decrease in N%, especially in HA, which is the expected SOM evolution in the Bh, resulting in a C/N greater than 45. In the BAR4 profile and the

497 BAR2 topsoil, the lower C/N and higher $\delta^{15}N$ indicate that the
498 lowering of the water table has resulted in a better oxygenation and N
499 supply from the topsoil, promoting microbial activity which
500 consumed C and increased ^{15}N (Kamer et al., 2003; Dijkstra et al.,
501 2006).
502
503 *3.2.3. Respiration kinetics*
504 Results of the modelling of the respiration data are given in Fig.
505 10. Topsoil horizons were characterized by a fast pool having a larger
506 relative size when hydromorphic (BAR3), and smaller when better
507 drained (BAR2 and BAR4). Well expressed E horizons (BAR2 and
508 BAR3) showed a large relative size of the fast pool and high
509 respirations rates in fast and slow pools. Bh horizons showed a low
510 relative size of the fast pool and low respiration rates of the slow
511 pool, consistent with high aromaticity and high C/N. In the BAR4
512 profile these latter characteristics were observed up to the topsoil,
513 indicating that over the entire profile the slow pool has not, or very
514 little, rejuvenated after truncation.
515 The respiration rates obtained here can be compared to respiration
516 rates obtained for other soils with similar methods at a temperature
517 comprised between 25 and 30° (Fig. 11). Yang et al. (2007), Haddix
518 et al. (2011) and Kern et al. (2019) provided data from topsoil
519 horizons of a variety of soil types from cold to hot, and humid to dry
520 climates; Lucas et al. (2020) provided data from topsoil and Bh
521 horizons of other Amazonian podzols. The respiration rates obtained
522 here are in the same range that those obtained for the topsoil of other
523 soil types regarding the fast pool, but lower regarding the slow pool.
524 For the latter, the respiration rate were in the range [$2.4\ 10^{-2}$ – $5.0\ 10^{-}$

525 ^{1}] y^{-1} for topsoil of other soil types, [2.4 10^{-3} – 1.8 10^{-2}] y^{-1} for topsoil
526 of untruncated podzols and [6.8 10^{-4} – 2.4 10^{-3}] y^{-1} for the Bh
527 horizons. The respiration rate of the Bh slow pool is therefore on
528 average about 2 orders of magnitude lower than that observed for the
529 topsoil of most soils.
530
531 *3.3. Carbon stock and soil genesis*
532
533 *3.3.1. Profile genesis*
534 The untruncated podzol profiles, where the water table has not
535 been lowered, store large amount of C (at least 67.9, 73.7 and 56.8 kg
536 C m^{-2} for profiles BAR1, -2 and -3, respectively). The average is 62.8
537 kg ha^{-1}, which is consistent with the results of previous studies
538 (Montes et al., 2012; Pereira et al., 2016; Doupoux et al., 2017). We
539 calculated the minimum time required to form the presently observed
540 BAR1, BAR2 and BAR3 profiles and the time required to reach 99%
541 of the observed ^{14}C age and Bh C pool, considering that these values
542 correspond to a steady state (Fig. 11 and Table 2). The calculations
543 gave a range of time according to assumptions about the size of the
544 fast Bh pool. The minimum time to form the profile is a lower bound
545 but not likely, because it corresponds to a scenario with no C outflux
546 from the Bh and in which the profile evolves very quickly (Fig. 12).
547 The time needed to reach 99% of the steady state gives a more
548 probable order of magnitude of the minimum genesis time. The
549 BAR4 profile was not considered because, truncated, it does not meet
550 the conditions of constant flux rates with time.
551 The order of magnitude of the time to reach 99% of steady state is
552 around 30000 y for the BAR1 and BAR2 profiles and around 50000

553 years for the BAR3 profile (Table 2). For the BAR2 and BAR3
554 profiles these times are certainly underestimated because the horizon
555 located beneath the Bh was not reached during the drilling so that the
556 Bh total C stock and therefore the genesis time were underestimated.
557 Regardless, these results are consistent with the late Pleistocene age
558 of the parent material and show that these podzols accumulated
559 organic carbon for a very long time.
560
561 **Table 2**
562 Carbon stock, apparent age and time required to form the profiles

Profile	P or A horizons		Bh horizon		Minimum time to form the profile (y)	Time to reach 99% of steady state (y)
	Carbon stock (kg m^{-2})	Apparent age (y BP)	Carbon stock (kg m^{-2})	Apparent age (y BP)		
BAR1	29.59	110	35.58	4785	9690 – 11400	29250 – 30380
BAR2	6.71	105	59.95	4689	9830 – 10550	28700 – 29400
BAR3	7.84	108	37.51	6699	14800 – 18260	48640 – 54215
BAR4	3.73	106	19.28			

563
564
565 *3.3.2. Soil OM dynamics after truncation*
566 How much and at what rate was the organic carbon of the BAR4
567 profile mineralized after truncation of the profile and corresponding
568 oxygenation of the Bh? To obtain an order of magnitude, the initial C
569 content of the BAR4 profile can be assumed to be the same as that
570 currently observed in the untruncated podzol, which will be
571 represented here by the average of the BAR2 and BAR3 profiles.
572 Measured respiration rates allow calculation of how long it takes to
573 decrease the C content of untruncated podzol to the BAR4 values and
574 how much C would be released into the atmosphere after the perched
575 groudwater disappears and oxygenated air enters the Bh. The

576 calculation was performed using the following equation, and the data
577 used for the calculation is given in Table 3.
578
579 $$C = C_0 \left(f_{Fp} \left(e^{-k_{Fp} t} \right) + \left(1 - f_{Fp} \right) \left(e^{-k_{Sp} t} \right) \right)$$
580
581 Where C is the carbon pool at time t, C_0 the initial carbon pool, f_{Fp}
582 the initial fast pool fraction, k_{Fp} and k_{Sp} the respiration rate of the fast
583 and the slow poll, respectively. The results are that it takes about 10
584 and 1220 y for topsoil horizon and Bh, respectively, to derive BAR4
585 values from untruncated podzol values. The latter seems consistent
586 with the rate of bank erosion by an Amazonian meander, estimated
587 at, in m y^{-1}, 0.008 to 0.015 of the meander width (Constantine et al.,
588 2014), which would give a displacement of 1 to 2 m y^{-1} for the
589 Demini meander. It should be noted, however, that the lateral
590 widening of the flood plain is slower than the displacement of a
591 meander (Camporeale et al., 2006).
592 Assuming that the disappearance due to climate change of the
593 permanent water-table perched above the Bh would have the same
594 consequence as what was observed in the topochronosequence, we
595 can extrapolate the measured mineralization rate to the Amazonian
596 podzol area. The carbon pools decrease being exponential, the
597 emission of C per year decreases over time: it is on average about 63
598 gC m^{-2} y^{-1} during the first 10 years, 54 gC m^{-2} y^{-1} during the
599 following 90 years and 41 gC m^{-2} y^{-1} during the following 400 years.
600 These values, related to the 155000 km² of the Amazonian podzol
601 area (Montes et al., 2011), would correspond to an emission of C into
602 the atmosphere about 9.8 10^{12}, 8.4 10^{12}, 6.3 10^{12} gC y^{-1} for the 0-10 y,

603 10-100 y, 100-500 y periods, respectively. These values, however,
604 remain low compared to current carbon emission by fossil fuels
605 (about 9 10^{15} g y^{-1}, IEA (2020)). It should also be noted that other
606 processes may arise after Bh oxygenation begins. Some can
607 accelerate degradation, such as the addition of nitrogen from the
608 surface horizons (Qiao et al., 2016) or fluctuating water content (Van
609 Gestel et al., 1993), others can slow it down, such as substrate
610 availability (Wei et al., 2015). **Table 3**
611 Data for calculation of SOM mineralization after truncation.
612 Untruncated podzol values are the average of values obtained for the
613 BAR2 and BAR3 profiles.

	C content		Fast pool fraction	Respiration rate (y^{-1})	
	kg m^{-2}	kg m^{-3}		Fast pool	Slow pool
Topsoil horizons					
Untruncated podzol	7.27	11.88	1.25 10^{-3}	7.70	1.01 10^{-2}
BAR4	3.73	10.68	5.04 10^{-3}	6.96	7.72 10^{-4}
Bh					
Untruncated podzol	48.73	19.43	1.25 10^{-3}	4.54	1.18 10^{-3}
BAR4	19.28	4.59	1.22 10^{-3}	7.08	6.76 10^{-4}

614
615

616 4. Conclusions

617

618 The studied topochronosequence comprised typical equatorial
619 giant podzol and equatorial hydromorphic podzols, both of which
620 with a perhumid Bh under reducing conditions. They store large
621 amounts of C (62.8 kg m^{-2} on average) and result from a long
622 genesis time the minimum estimate of which is around 10-20 ky, but
623 which is very probably greater than 30-50 ky. The organic matter of
624 topsoil had a rapid average turnover, about 100 y, therefore likely to
625 mineralize very quickly in the event of a change towards a drier

626 climate. In the Bh of these podzols, increased OM age was related to
627 increased heavy fraction, aromaticity, C/N and $\delta^{13}C$. The H_{LIFS}
628 humification index was found to be inappropriate for these soils, due
629 to interference with the soil colour.
630 The lowering of the water table in part of the topochronosequence
631 and the subsequent oxygenation of the Bh resulted in a decrease in
632 the Bh C stock from about 19 kgC m^{-3} to 5 kgC m^{-3} that requires,
633 according to measured respiration rates, a duration of around 1200 y.
634 Applying these respiration rates to the Bh oxygenation that would
635 result from climate change gives a rough estimate of subsequent C
636 emission, around 55 gC m^{-2} y^{-1} on average during the first 100 years.
637 Extrapolated to all Amazonian podzols, and regardless of other
638 processes that may be involved, this value would correspond to 8.5
639 10^{12} gC y^{-1}.
640
641

642 ## CRediT authorship contribution statement

643

644 **Célia R. Montes:** Conceptualization, Methodology, Writing -
645 Original Draft, Investigation, Supervision, Project administration,
646 Funding acquisition. **Patricia Merdy:** Methodology, Formal
647 analysis, Writing – review & Editing. **Wilson T.L. da Silva:**
648 Investigation, Supervision. **Débora Ishida:** Investigation,
649 Ressources. **Adopho J. Melfi:** Investigation, Writing – review &
650 Editing. **Roberta C. Santin:** Investigation. **Yves Lucas:**
651 Conceptualization, Methodology, Data Curation, Writing - Original
652 Draft, Supervision, Project administration, Funding acquisition.

Declaration of Competing Interest

The authors declare that they have no known competing financial interests or personal relationships that could have appeared to influence the work reported in this paper.

Funding

This work was supported by the São Paulo Research Foundation (FAPESP) [grants numbers #2011/03250-2; #2012/51469-6, doctoral scholarship #2012/18092-6]; the National Council for Scientific and Technological Development (CNPq) [research scholarship to CRM #303478/2011-0; #306674/2014-9]; and French Agence Nationale de la Recherche (ANR) [grant number ANR-12-IS06-0 0 02 “C-PROFOR”].

Appendix A. Supplementary data

References

Adeney, J.M., Christensen, N.L., Vicentini, A., Cohn-Haft, M., 2016. White-sand ecosystems in Amazonia. Biotropica 48, 7-23. https://doi.org/10.1111/btp.12293.

679 Anderson, A.B., 1981. White-sand vegetation of Brazilian Amazonia.
680 Biotropica 13, 199–210. https://doi.org/10.2307/2388125
681 Bardy, M., Derenne, S., Allard, T., Benedetti, M. F., Fritsch, E.,
682 2011. Podzolisation and exportation of organic matter in black
683 waters of the Rio Negro (upper Amazon basin, Brazil).
684 Biogeochem. 106, 71–88. https://doi.org/10.1007/s10533-010-
685 9564-9
686 Birch, H.F., 1958. The effect of soil drying on humus decomposition
687 and nitrogen availability. Plant Soil 10, 9–31.
688 https://doi.org/10.1007/BF01343734
689 Cadisch, G., Imhof, H., Urquiaga, S., Boddey, R.M., Giller, K.E.,
690 1996. Carbon turnover ($\delta^{13}C$) and nitrogen mineralization
691 potential of particulate light soil organic matter after rainforest
692 clearing. Soil Biol. Biochem. 28, 1555-1567.
693 https://doi.org/10.1016/S0038-0717(96)00264-7
694 Camporeale, C., Perona, P., Porporato, A., Ridolfi, L.U.C.A., 2007.
695 Hierarchy of models for meandering rivers and related
696 morphodynamic processes. Rev. Geophys. 45, RG1001.
697 https://doi.org/10.1029/2005RG000185.
698 Christensen B.T., 2001. Physical fractionation of soil and structural
699 and functional complexity in organic matter turnover. Eur. J.
700 Soil Sci. 52, 345-353. https://doi.org/10.1046/j.1365-
701 2389.2001.00417.x
702 Constantine, J.A., Dunne, T., Ahmed, J., Legleiter, C., Lazarus, E.D.,
703 2014. Sediment supply as a driver of river meandering and
704 floodplain evolution in the Amazon Basin. Nature Geoscience 7,
705 899-903. https://doi.org/10.1038/NGEO2282

706 Cremon, E.H., Rossetti, D.F. and Zani, H., 2012. Gênese e evolução
707 geomorfológica do megaleque Demini (norte da Amazônia)
708 baseado na análise morfoestrutural e hidroperíodo. Anais 9°
709 SINAGEO, 2012, Rio de Janeiro.
710 http://www.sinageo.org.br/2012/trabalhos/2/2-440-165.html
711 (accessed 21 October 2020).
712 Dijkstra, P., Ishizu, A., Doucett, R., Hart, S.C., Schwartz, E.,
713 Meyailo, O.V., Hungate, B.A., 2006. ^{13}C and ^{15}N natural
714 abundance of the soil microbial biomass. Soil Biol. Biochem.
715 38, 3257-3266. https://doi.org/10.1016/j.soilbio.2006.04.005
716 Dubroeucq, D., Volkoff, B., 1998. From oxisols to spodosols and
717 histosols: evolution of the soil mantles in the Rio Negro Basin
718 (Amazonia). Catena 32, 245-280. https://doi.org/10.1016/S0341-
719 8162(98)00045-9
720 Doupoux, C., Merdy, P., Montes, C.R., Nunan, N., Melfi, A.J.,
721 Pereira, O.J.R., Lucas, Y., 2017. Modelling the genesis of
722 equatorial podzols: age and implications for carbon fluxes,
723 Biogeosciences 14, 2429–2440. https://doi.org/10.5194/bg-14-
724 2429-2017.
725 García-Villacorta, R., Dexter, K.G., Pennington, T., 2016.
726 Amazonian white-sand forests show strong floristic links with
727 surrounding oligotrophic habitats and the Guiana Shield.
728 Biotropica 48, 47-57. https://doi.org/10.1111/btp.12302.
729 Gutiérrez, J.M., R.G. Jones, G.T. Narisma, L.M. Alves, M. Amjad,
730 I.V. Gorodetskaya, M. Grose, N.A.B. Klutse, S. Krakovska, J.
731 Li, D. Martínez-Castro, L.O. Mearns, S.H. Mernild, T. Ngo-
732 Duc, B. van den Hurk, and J.-H. Yoon, 2021: Atlas. In Climate
733 Change 2021: The Physical Science Basis. Contribution of

Working Group I to the Sixth Assessment Report of the Intergovernmental Panel on Climate Change [Masson-Delmotte, V., P. Zhai, A. Pirani, S.L. Connors, C. Péan, S. Berger, N. Caud, Y. Chen, L.Goldfarb, M.I. Gomis, M. Huang, K. Leitzell, E. Lonnoy, J.B.R. Matthews, T.K.Maycock, T. Waterfield, O. Yelekçi, R. Yu, and B. Zhou (eds.)]. Cambridge University Press. In Press. Interactive Atlas available from Available from http://interactive-atlas.ipcc.ch/

Haddix, M.L., Plante, A.F., Conant, R.T., Six, J., Steinweg, J.M., Magrini-Bair, K., Drijber, R.A., Morris, S.J., Paul, E.A., 2011. The role of soil characteristics on temperature sensitivity of soil organic matter. Soil Sci. Soc. Am. J. 75, 56-68. https://doi.org/10.2136/sssaj2010.0118

IBGE, 2011. Diretoria de Geociências (DGC). Coordenação de Recursos Naturais e Estudos Ambientais (CREN). Mapas georeferencias de recursos naturais. Escala 1: 250:000, formato digital: shp. Rio de Janeiro, 2008. ftp://geoftp.ibge.gov.br/informacoes_ambientais/geologia/levantamento_geologico/mapas/unidades_da_federacao/am_geologia.pdf/ (accessed 21 October 2020).

IEA, 2020. Global CO2 emissions in 2019, IEA, Paris. https://www.iea.org/articles/global-co2-emissions-in-2019/ (accessed 21 October 2020).

Ishida, D.A., Montes, C.R., Lucas, Y., Pereira, O.J.R., Merdy, P., Melfi, A.J., 2014. Genetic relationships between ferralsols, podzols and white kaolin in Amazonia. Eur. J. Soil Sci. 65, 706-717. https://doi.org/10.1111/ejss.12167

Iturbide, M., Fernández, J., Gutiérrez, J.M., Bedia, J., Cimadevilla, E., Díez-Sierra, J., Manzanas, R., Casanueva, A., Baño-Medina, J., Milovac, J., Herrera, S., Cofiño, A.S., San Martín, D., García-Díez, M., Hauser, M., Huard, D., Yelekci, Ö., 2021. Repository supporting the implementation of FAIR principles in the IPCC-WG1 Atlas. Zenodo, DOI: 10.5281/zenodo.3691645. Available from: https://github.com/IPCC-WG1/Atlas

Kaiser, K., Zech, W., 2000. Dissolved Organic Matter sorption by mineral constituents of subsoil clay fractions. J. Plant Nutr. Soil Sci. 163, 531–535. https://doi.org/10.1002/1522-2624(200010)163:5<531::AID-JPLN531>3.3.CO;2-E.

Kern, J., Giani, L., Teixeira, W., Lanza, G., Glaser, B., 2019. What can we learn from ancient fertile anthropic soil (Amazonian Dark Earths, shell mounds, Plaggen soil) for soil carbon sequestration? Catena, 172, 104-112. https://doi.org/10.1016/j.catena.2018.08.008

Kramer, M.G., Sollins, Ph., Sletten, R.S., Swart, P.K., 2003. N isotope fractionation and measures of organic matter alteration during decomposition. Ecology 84, 2021-2025. https://doi.org/10.1890/02-3097

Leenheer, J.A., 1980. Origin and nature of the humic substances in the waters of the Amazon River basin. Acta Amazonica 10, 513–526. https://doi.org/10.1590/1809-43921980103513

Lucas, Y., Boulet, R., Veillon, L., 1987. Systèmes sols ferrallitiques - podzols en région amazonienne. In Righi, D., Chauvel, A. (Eds.), Podzols et Podzolisation. AFES, Plaisir and INRA, Paris, pp. 53-65.

Lucas, Y., Montes, C.R., Mounier, S., Loustau-Cazalet, D., Ishida, D., Achard, R., Garnier, C. Melfi, A.J., 2012. Biogeochemistry of an amazonian podzol-ferralsol soil system with white kaolin. Biogeoscience 9, 3705-3720. https://doi.org/10.5194/bg-9-3705-2012

Lucas Y., 2001. The role of the plants in controlling rates and products of weathering: importance of the biological pumping. Ann. Rev. Earth Planet. Sci. 29, 35-163. https://doi.org/10.1146/annurev.earth.29.1.135

Lucas, Y., Nahon, D., Cornu, S., Eyrolle, F., 1996. Genèse et fonctionnement des sols en milieu équatorial. C . R. Acad. Sci. Paris Ser. IIA 322, 1-16. http://horizon.documentation.ird.fr/exl-doc/pleins_textes/pleins_textes_6/b_fdi_43-44/010004553.pdf

Lucas Y., Santin R.C., Silva W.T.L. da, Merdy P., Melfi A.J., Pereira O.J.R., Montes C.R., 2020. Soil sample conservation from field to lab for heterotrophic respiration assessment. MethodsX 7, 101039. https://doi.org/10.1016/j.mex.2020.101039

Marques, J.D.D.O., Luizão, F.J., Teixeira, W.G., Vitel, C.M., Marques, E.M.D.A., 2016. Soil organic carbon, carbon stock and their relationships to physical attributes under forest soils in central Amazonia. Revista árvore 40, 197-208.

Marques, J.D.O., Luizão, F., Teixeira, W., Nogueira, E., Fearnside, P., Sarrazin, M., 2017. Soil carbon stocks under Amazonian forest: distribution in the soil fractions and vulnerability to emission. Open J. Forest. 7, 121-142. https://doi.org/10.4236/ojf.2017.72008.

Merdy, P., Lucas, Y., Coulomb, B., Melfi, A.J., Montes, C.R., 2021. Soil organic carbon mobility in equatorial podzols: soil column

816 experiments. Soil 7, 585–594. https://doi.org/10.5194/soil-7-
817 585-2021.
818 Miller, A.E., Schimel, J.P., Meixner, T., Sickman, J.O., Melack,
819 J.M., 2005. Episodic rewetting enhances carbon and nitrogen
820 release from chaparral soils. Soil Biol Biochem. 37, 2195–2204.
821 https://doi.org/10.1016/j.soilbio.2005.03.021
822 Milori, D.M.B.P., Martin-Neto, L., Bayer, C., Mielniczuk, J.,
823 Bagnato, V.S., 2002. Humification degree of soil humic acids
824 determined by fluorescence spectroscopy. Soil Sci. 167, 739-
825 749. https://doi.org/10.1097/00010694-200211000-00004
826 Milori, D.M.B.P, Galeti, H.V.A, Martin-Neto, L., Dieckow, J., Pérez,
827 M.G., Bayer, C., Salton, J., 2006. Organic matter study of whole
828 soil samples using laser-induced fluorescence spectroscopy. Soil
829 Sci. Soc. Am. J. 70, 57–63.
830 https://doi.org/10.2136/sssaj2004.0270
831 Montes, C.R., Lucas, Y., Pereira, O.J.R., Achard, R., Grimaldi, M.,
832 Melfi, A.J., 2011. Deep plant-derived carbon storage in
833 Amazonian podzols. Biogeosciences 8, 113-120.
834 https://doi.org/10.5194/bg-8-113-2011
835 Munsell, 1990. Munsell soil color chart, Kollmorgen Instruments
836 Corp., New York.
837 Paul, E.A., Morris, S.J., Bohm, S., 2001. The determination of soil C
838 pool sizes and turnover rates: biophysical fractionation and
839 tracers. In: Lal, R., Kimble, J.M., Follet, R.F., Stewart, B.A.
840 (Eds.), Assessment Methods for Soil Carbon, Lewis Publishes,
841 Boca Raton, pp. 193–206 .
842 Pereira, O.J.R., Montes, C.R., Lucas, Y., Santin, R.C., Melfi, A.J.,
843 2015. A multi-sensor approach for mapping plant-derived

carbon storage in Amazonian podzols. Int. J. Rem. Sens. 36, 2076-2092. http://dx.doi.org/10.1080/01431161.2015.1034896

Pereira, O.J.R., Montes, C.R., Lucas, Y., Melfi, A.J., 2016. Evaluation of pedotransfer equations to predict deep soil carbon stock in tropical Podzols compared to other soils of Brazilian Amazon forest. In: Digital Soil Morphometrics, A.E. Hartemink and B. Minasny (eds.), Chap. 21 (pp. 331-349), Series: Progress in Soil Science, Springer. https://doi.org/10.1007/978-3-319-28295-4_21

Qiao, N., Xu, X., Hu, Y., Blagodatskaya, E., Liu, Y., Schaefer, D., Kuzyakov, Y., 2016. Carbon and nitrogen additions induce distinct priming effects along an organic-matter decay continuum. Scientific Reports 6, 1-8. https://doi.org/10.1038/srep19865.

Reboita, M.S., Gan, M.A., Rocha, Rosmeri, P. da, Ambrizzi, T., 2010. Regimes de precipitação na América do Sul: uma revisão bibliográfica. Rev. Bras. Meteorol. 25, 185-204. https://dx.doi.org/10.1590/S0102-77862010000200004

Reis, N.J., Almeida, M.E., Riker, S.L., Ferreira, A.L., 2006. Geologia e Recursos Minerais do Estado do Amazonas. CPRM – Serviço Geológico do Brasil, maps and notice, 125p.

Scheinost, A.C., Chavernas, A., Barrón, V., Torrent, J., 1998. Use and limitations of second-derivative diffuse reflectance spectroscopy in the visible to near-infrared range to identify and quantify Fe oxide minerals in soils.

Sohi, S.P., Mahieu, N., Arah, J.R.M., Powlson, D.S., Madari, B., Gaunt, J.L., 2001. A procedure for isolating soil organic matter

fractions suitable for modeling. Soil Sci. Soc. Am. J. 65, 1121–1128. https://doi.org/10.2136/sssaj2001.6541121x

Swift, R., 1996. Organic matter characterization. In: Sparks, D.L., Page, A.L., Helmke, P.A., Loeppert, R.H., Soltanpour, P.N., Tabatabai, M.A., Johnson, C.T., Sumner, M.E. (eds), Methods of soil analysis, Part 3: chemical methods. SSSA Book Series N°5, SSSA and ASA, Madison, WI, 1011–1069. https://doi.org/10.2136/sssabookser5.3.c35

Tadini, A.M., Nicolodelli, G., Senesi, G.S., Ishida, D.A., Montes, C.R., Lucas, Y., Mounier, S., Guimarães, F.E.G., Milori, D.M.B.P., 2018. Soil organic matter in podzol horizons of the Amazon region: Humification, recalcitrance, and dating. Sci. Tot. Environ. 613-614, 160-167. https://doi.org/10.1016/j.scitotenv.2017.09.068

Tardy, Y., Roquin, C., Bustillo, V., Moreira, M., Martinelli, L.A., Victoria, R., 2009. Carbon and Water Cycles, Amazon River Basin, Applied Biogeochemistry. Atlantica, Biarritz.

Trumbore, S., 2000. Age of soil organic matter and soil respiration: radiocarbon constraints on belowground C dynamics. Ecol. Appl. 10, 399-411. https://doi.org/10.1890/1051-0761(2000)010[0399:AOSOMA]2.0.CO;2.

Van Gestel, M., Merckx, R., Vlassak, K., 1993. Microbial biomass and activity in soils with fluctuating water contents. In Soil Structure/Soil Biota Interrelationships, Elsevier, pp. 617-626. https://doi.org/10.1016/B978-0-444-81490-6.50050-9.

Wei, H., Chen, X., Xiao, G., Guenet, B., Vicca, S., Shen, W., 2015. Are variations in heterotrophic soil respiration related to changes in substrate availability and microbial biomass carbon in the

subtropical forests? Scientific Reports 5, 1-11. https://doi.org/10.1038/srep18370.

Yang, L., Pan, J., Shao, Y., Chen, J. M., Ju, W. M., Shi, X., Yuan, S., 2007. Soil organic carbon decomposition and carbon pools in temperate and sub-tropical forests in China. J. Env. Manag. 85, 690-695. https://doi.org/10.1016/j.jenvman.2006.09.011

905 **Fig. 1**

906

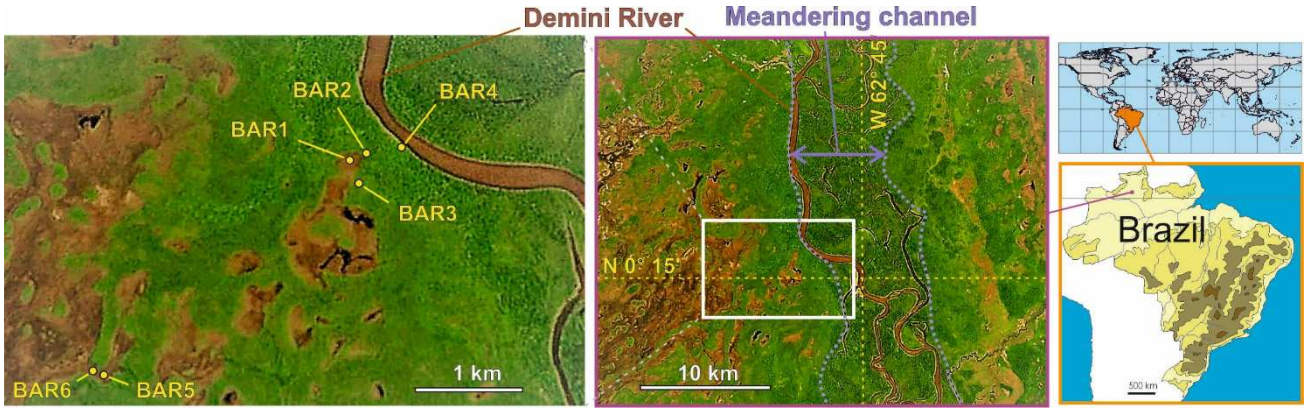

908

909

910 **Fig. 2**

911

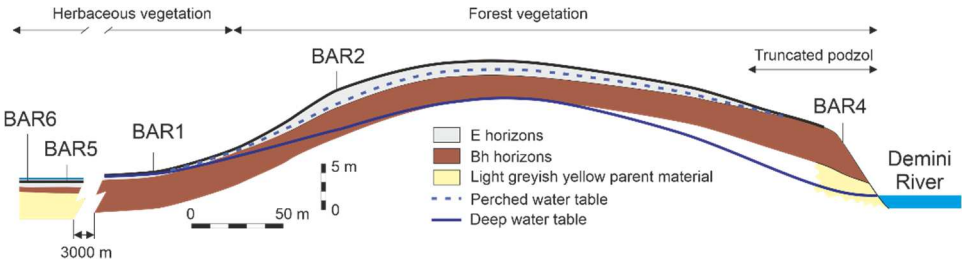

912

913

914

915 **Fig. 3**

916

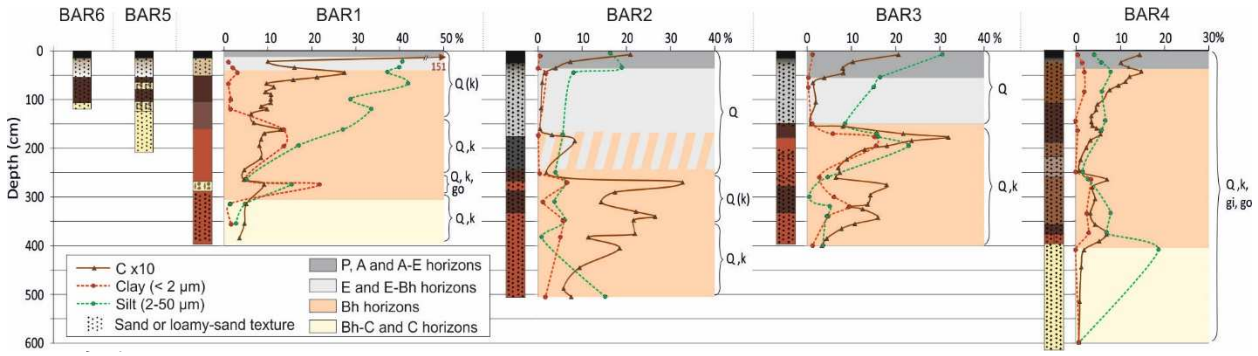

918

919

920 **Fig. 4**

921

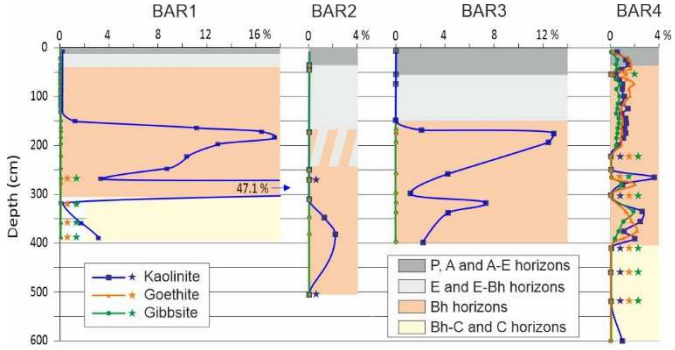

922

923

924

925 **Fig. 5**

926

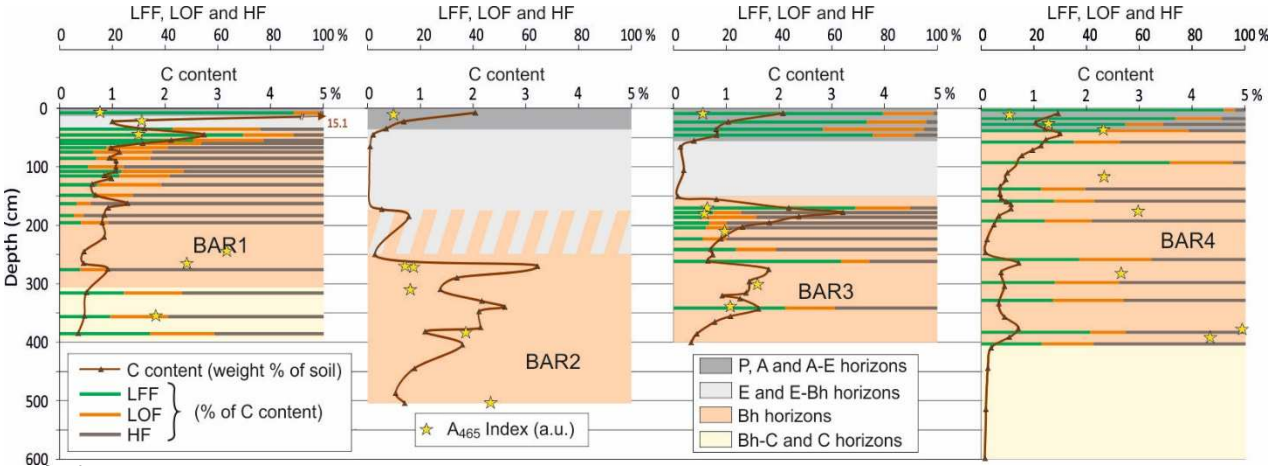

928

929

930

931

932 **Fig. 6**

933

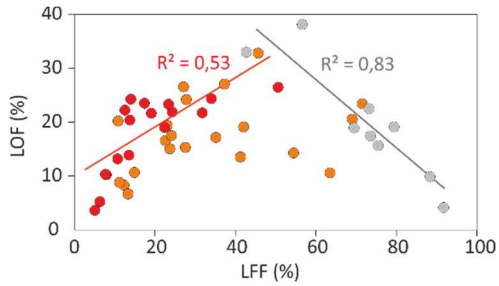

934

935

936

937 **Fig. 7**

938

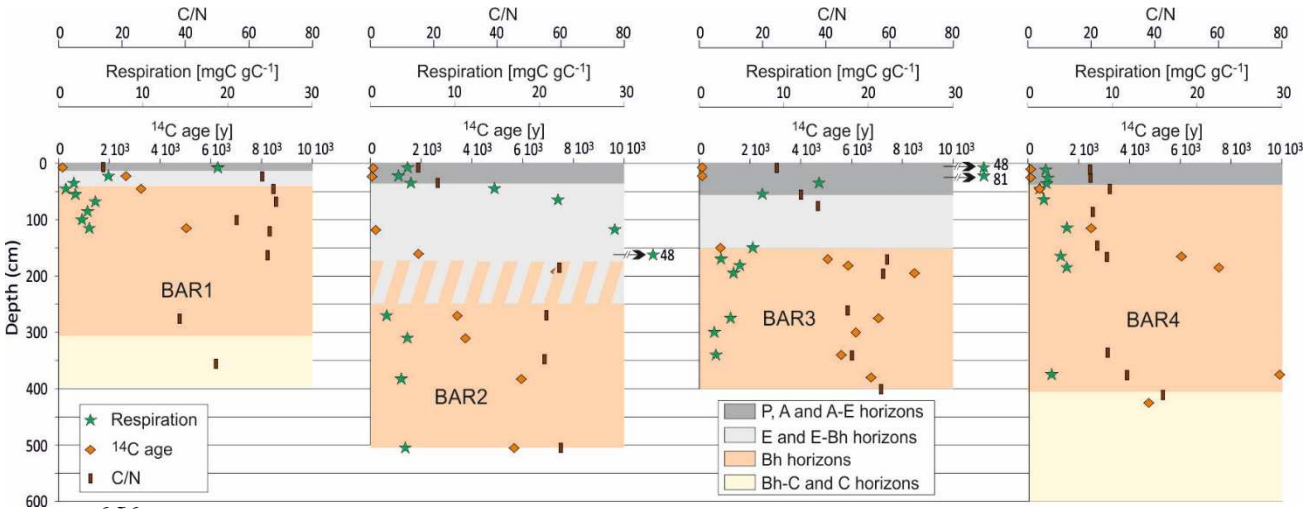

940

941

942

943 **Fig. 8**

944

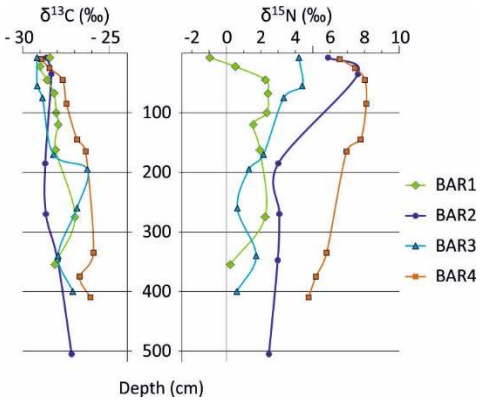

945

946

947

948 **Fig. 9**

949

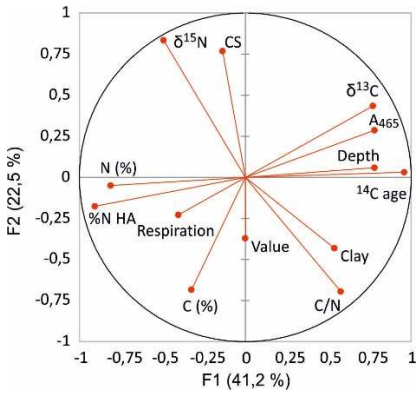

950

951

952

953

954 **Fig. 10**

955

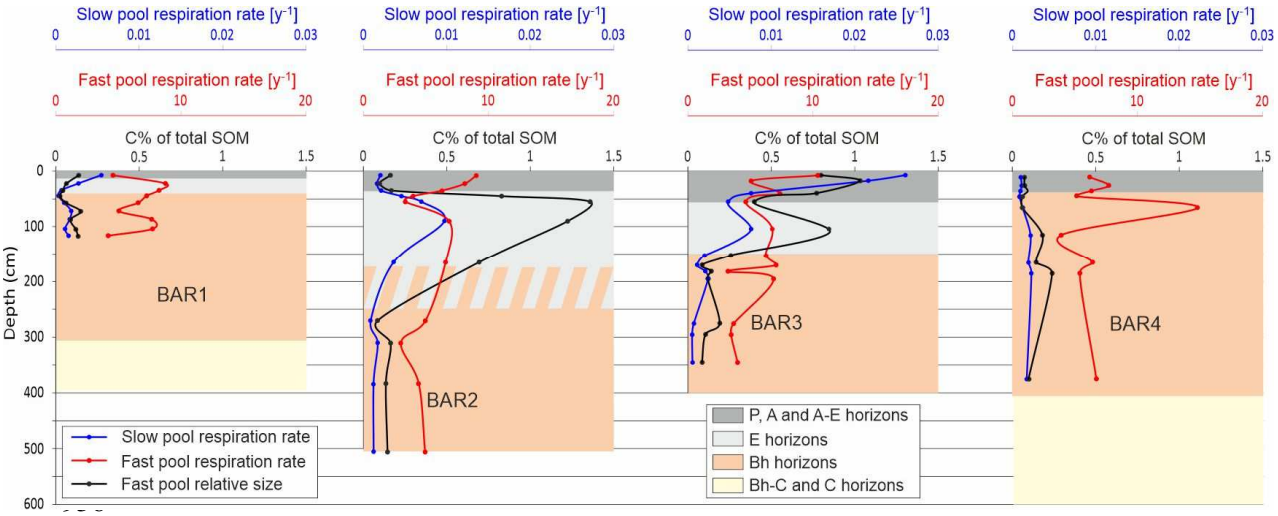

957

958

959 **Fig. 11**

960

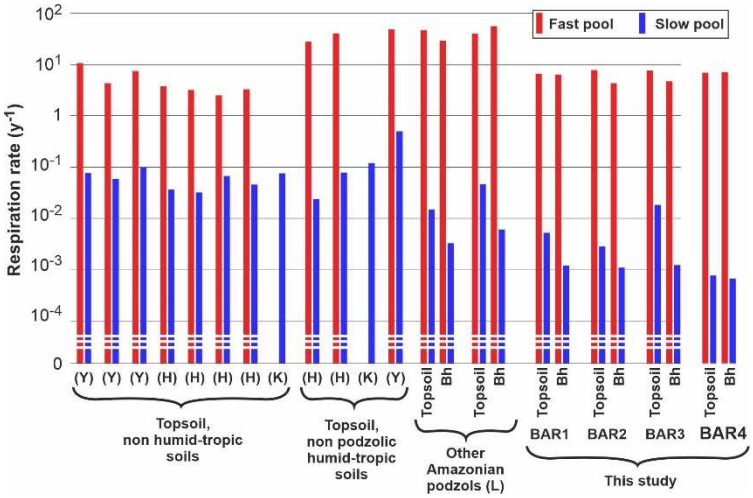

961

962

963

964 **Fig. 12**

965

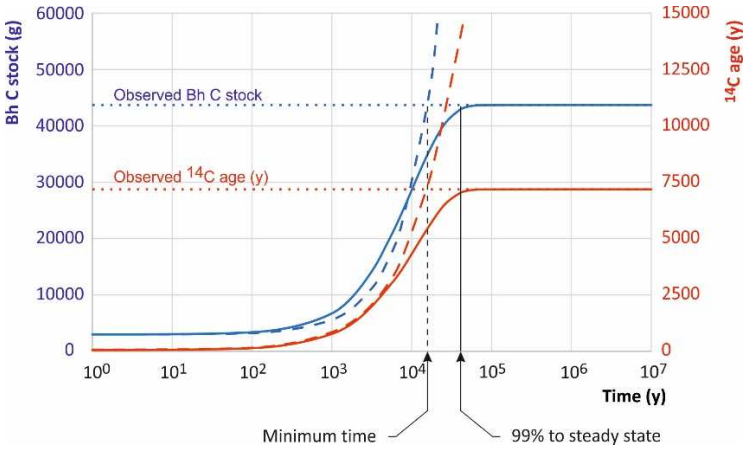

966

967

968

Figure caption

Fig. 1. Location of the studied site

Fig. 2. Situation of the soil profiles with regard to topography and sketch of the horizon geometry.

Fig. 3. The studied profiles: borehole logs (colours seek to reflect actual colours); C (carbon), clay and silt in %; mineralogy. Q: quartz, k: kaolinite, gi: gibbsite, go: goethite (uppercase: dominant mineral; lowercase in parentheses: trace mineral only). E-Bh horizons: transition between E and Bh horizons; Bh-C horizons: transition between Bh and C horizons.

Fig. 4. Quantifiable kaolinite, goethite and gibbsite in the BAR1 to BAR4 profiles. A star indicates that the given mineral has been identified but in a quantity too small to be quantified.

Fig. 5. Organic matter fractionation and A_{465} humification index. LFF: light free fraction, LOF: light occluded fraction, HF: heavy fraction.

Fig. 6. Relationships between LFF and LOF % in SOM. Grey points: P, A and A-E horizons; red and orange points: Bh and B-C horizons. Red points refer to the BAR1 profile.

995 **Fig. 7.** SOM apparent ^{14}C age, C/N values and cumulative
996 respiration at 660 days.
997
998 **Fig. 8.** SOM isotopic data
999
1000 **Fig. 9.** PCA correlation circles on the first two factorial axes.
1001 Percent on each factorial axis gives the explained variance. Value:
1002 value of the horizon Munsell color; %N HA: % of N in the extracted
1003 humic acid fraction of the SOM (data from Tadini et al., 2018). CS:
1004 coarse sand.
1005
1006 **Fig. 10.** Relative size of the SOM fast pool (C% of the total SOM)
1007 and respiration rates of the slow and fast pool.
1008
1009 **Fig. 11.** Respiration rates of fast and slow pools of soil organic
1010 matter. (Y): Yang et al., 2007; (H): Haddix et al., 2011; (K) : Kern et
1011 al., 2019 ; (L): Lucas et al., 2020.
1012
1013 **Fig. 12.** Modelling the time of genesis. Dashed lines: scenario for
1014 minimum time; plain lines: scenario for steady state.
1015

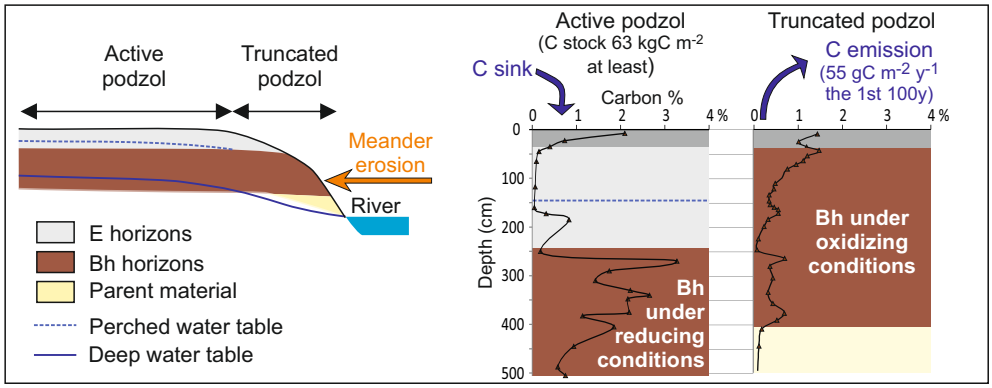
Active podzol
Truncated podzol
Meander erosion
River
E horizons
Bh horizons
Parent material
Perched water table
Deep water table
Active podzol
(C stock 63 kgC m-2 at least)
C sink
Carbon %
Truncated podzol
C emission
(55 gC m-2 y-1 the 1st 100y)
Depth (cm)
Bh under reducing conditions
Bh under oxidizing conditions